Preprints of the 19th World Congress
The International Federation of Automatic Control
Cape Town, South Africa. August 24-29, 2014

Constrained Iterative Feedback Tuning for Robust High-Precision Motion Control

Bart J.C.H. Van der Velden * **Tom Oomen** * **Marcel F. Heertjes** *,**

* *Control Systems Technology Group, Department of Mechanical Engineering, Eindhoven University of Technology, Eindhoven, The Netherlands (e-mail corresponding author: m.f.heertjes@tue.nl).*
** *Mechatronics Technology Development, ASML, Veldhoven, The Netherlands.*

Abstract: The aim of this paper is to extend iterative feedback tuning (IFT), which is a data-based approach for controller tuning, with robustness constraints. Hereto a constrained IFT problem is formulated that is solved by introducing a penalty function. Essentially, the gradient estimates decompose into (a) the well-known IFT gradients and (b) the gradients with respect to this penalty function. Experimental results obtained from the motion control systems of an industrial wafer scanner confirm enhanced performance with guaranteed robustness properties.

1. INTRODUCTION

Control systems are designed by using either model-based approaches or data-based approaches. Model-based approaches refer to the system first being modeled, often through the aid of system identification. Modeling, however, is usually a time-consuming and difficult process. In this regard, data-based approaches are appealing since they avoid the need for modeling and enable the direct tuning of the controller based on measurement data. This has led to a variety of data-based control design methods, including unfalsified control [Safonov and Tsao, 1997], virtual reference feedback tuning [Campi et al., 2002], and iterative feedback tuning, which is abbreviated as IFT [Hjalmarsson et al., 1994, Hjalmarsson, 2002]. Interestingly, in Hjalmarsson [2005] it is shown that many of the data-based approaches can be interpreted as being model-based, except for IFT. IFT is an iterative optimization approach that aims at obtaining unbiased gradient estimates by conducting multiple experiments. In a gradient-based update scheme, the gradient estimates are used to compute a new set of controller parameters. The optimal set of parameters associates with a minimum of a performance-relevant cost function in time domain. IFT has been successfully applied in many applications, including process industry [Gevers, 2002], robotics [Kostić, 2004, Rico et al., 2012], mechatronics [Al Mamun et al., 2007, Liu et al., 2011], and stage control [Yang and Koo, 2013].

An important field of application where data-based controller tuning is appealing is in high-precision motion control. For feed-forward control design, model-based approaches have led to limited performance enhancements due to model uncertainty [Boerlage et al., 2003]. This has led to the development of data-based approaches in Van der Meulen et al. [2008] and Heertjes et al. [2010] for the multivariable case, which induce significant performance enhancements. It has recently been shown in Boeren and Oomen [2013] that the IFT algorithm employed in Van der Meulen et al. [2008] for feed-forward control has a direct system identification interpretation, see also Oomen et al. [2014]. In fact, the IFT algorithm deals with a closed-loop identification problem, but comes at the expense of efficiency. In Boeren and Oomen [2013], more efficient algorithms have been proposed rendering the use of IFT superfluous for feed-forward control design. Feedback design seems more suited for IFT, however. This is because (a) IFT requires no parametric system model, (b) unlike model-based synthesis algorithms IFT can deal with a predefined controller structure, and (c) control performance is optimized for the disturbance situation at hand so no disturbance model is needed.

Despite these clear advantages, a direct IFT implementation suffers from robustness issues as there are no guarantees that the closed-loop system remains stable during the iterations. This is evidenced by the development of IFT algorithms that take into account robust stability, see for example Prochazka et al. [2005], Veres and Hjalmarsson [2002]. These algorithms typically use approximations of robustness measures, including the ν-gap metric and $\mathscr{H}_\infty$ norms of relevant closed-loop transfer functions, which may be rather conservative. Moreover, strong guarantees for robust stability are not provided.

The main contribution of this paper is a new approach for constrained IFT. Additionally, the effectiveness of the approach will be tested through experimental results obtained from the high-precision motion systems of an industrial wafer scanner. To ensure robustness, a frequency-domain constraint is added to the objective function that represents the robustness objective. For the considered class of motion systems, non-parametric frequency response function models are relatively inexpensive, fast, and accurate to obtain. Although not directly usable for controller synthesis, these models are well-suited to evaluate robustness margins such as the modulus margin.

The central idea in this paper is to include a constraint, e.g., the modulus margin, in the optimization criterion. By means of a penalty function, the gradient-based IFT scheme decomposes into (a) the well-known IFT gradients and (b) the gradients with respect to this penalty function. This is related to the work of Hansson et al. [1999] where an interior-point method is adopted to take into account signal constraints on the input. In our approach, the numerical differentiation is done off-line based on the identified non-parametric model. During off-line optimization, a modified optimal set of controller parameters is obtained that satisfies the frequency-domain robustness specifications. With this set, a new IFT experiment is performed. Given the accuracy of the non-parametric model, it is fair to assume that no experiments are done that involve (significant) violations of the frequency domain robustness specifications, i.e. no controllers are implemented that possibly lead to unstable control design. This is important for high-precision motion systems like wafer scanners where machine damage should be avoided at all

times, but also for example for stages in electron microscopes, or component mounters in pick-and-place machinery.

The remainder of the paper is organized as follows. In Section 2, we will discuss IFT in the context of stage systems, then introduce the penalty function approach as a means to impose frequency-domain specifications, and discuss the extended optimization algorithm underlying this approach. In Section 3, simulation results with a 4th order stage model and experimental results on an industrial wafer stage system will be presented. In Section 4, a summary will be given of the main conclusions.

2. CONSTRAINED ITERATIVE FEEDBACK TUNING

Constrained iterative feedback tuning is presented as a means to impose frequency-domain specifications on the closed-loop stage system. First, the stage system context will be explained. Second, an overview of the IFT algorithm will be given that includes an extra iteration loop to penalize violations of the robustness specifications. Third, the derivation of the unbiased gradient estimates obtained from the IFT experiments will be discussed. Fourth, the derivation of the gradients with respect to the penalty function will be presented.

2.1 Stage System Context

Consider the stage controller structure in Fig. 1 where the linear

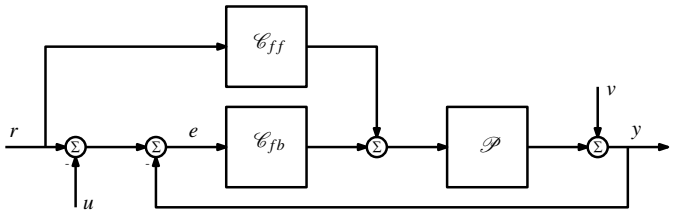

Fig. 1. Block diagram of the stage controller structure.

time-invariant stage system $\mathscr{P}$ has output y which is corrupted by the unmeasured disturbances v. These disturbances are assumed to be stochastic and uncorrelated with the other inputs r and u. Moreover, $\mathscr{P}$ is assumed to be single-input single-output and is controlled by a linear time-invariant feed-forward controller $\mathscr{C}_{ff}$ and feedback controller $\mathscr{C}_{fb}$. In this paper, $\mathscr{C}_{fb}$ is a function of the controller parameters $\rho = [\rho(1)\dots\rho(m)]^{\mathrm{T}}$ to be optimized, i.e. $\mathscr{C}_{fb} = \mathscr{C}_{fb}(\rho)$, with the number of parameters $m \geq 1$. In conducting point-to-point motion, tracking performance is reflected by the closed-loop error $e = r - u - y$, i.e. the difference between the reference command r, the output y, and an auxiliary input u used for the second IFT experiment only. The latter will be explained in more detail in Section 2.3.

2.2 IFT overview

IFT will be used to find the optimal set of controller parameters ρ^* that minimizes the cost function $J_e = J_e(\rho)$,

$$J_e = \frac{1}{2N}\mathbf{e}^T\mathbf{e}, \tag{1}$$

with the data sampled signal $\mathbf{e} = [e(1)\dots e(N)]^{\mathrm{T}}$, $\mathbf{e} = \mathbf{e}(\rho)$, and the number of samples $N > 0$, under the constraint

$$g \leq 0, \tag{2}$$

with $g = g(\rho)$ defined by

$$g(\rho) = \max_{\omega}\left(|\mathscr{S}(\omega,\rho)| - \mathscr{S}_b(\omega)\right). \tag{3}$$

Note that the particular choice of g in (3) is made to facilitate the exposition. The theory that will be presented is general and can be applied to other choices of g. $\mathscr{S} = \mathscr{S}(\omega,\rho)$ is the closed-loop sensitivity function which in frequency domain reads:

$$\mathscr{S}(z) = \frac{1}{1+\mathscr{C}_{fb}(z)\mathscr{P}(z)}, \tag{4}$$

with z^{-1} the unit-delay operator, whereas $\mathscr{S}_b = \mathscr{S}_b(\omega) > 0$ is a frequency-dependent function that for each frequency ω specifies the amplitude constraints imposed on $\mathscr{S}$.

To transform the above-described constrained optimization problem into an unconstrained problem, the cost function in (1) is extended with a penalty $J_g = J_g(\omega,\rho)$ that is based on the constraint function in (3), or

$$J_g = \frac{1}{2}\phi(g)g^2, \tag{5}$$

with piecewise linear function

$$\phi(g) = \begin{cases} 0, \text{ if } g \leq 0 \\ 1, \text{otherwise.} \end{cases} \tag{6}$$

With (1) and (5), define the cost function $J = J(\omega,\rho)$ as

$$J = J_e + \alpha J_g, \tag{7}$$

with $\alpha > 0$ a scaling factor. Equation (7) gives rise to the following unconstrained optimization problem:

$$\rho^* = \min_{\rho} J, \tag{8}$$

which can be solved iteratively using the Gauss-Newton algorithm:

$$\rho_{i+1} = \rho_i - \gamma_i H^{-1}\left.\frac{\partial J}{\partial \rho}\right|_{\rho=\rho_i}, \tag{9}$$

where $0 < \gamma_i \leq 1$ is the step size at iteration i, the gradient $\partial J/\partial\rho$ given by

$$\begin{aligned}\frac{\partial J}{\partial \rho} &= \frac{\partial J_e}{\partial \rho} + \alpha\frac{\partial J_g}{\partial \rho} \\ &= \frac{1}{N}\frac{\partial \mathbf{e}^T}{\partial \rho}\mathbf{e} + \alpha\phi(g)g\Bigg(\underbrace{\frac{\partial \phi(g)}{\partial g}\frac{\partial g}{\partial \rho}}_{0}g + \phi(g)\frac{\partial g}{\partial \rho}\Bigg),\end{aligned} \tag{10}$$

and the approximation of the Hessian $H = H(\rho)$ given by

$$H = \underbrace{\frac{1}{N}\frac{\partial \mathbf{e}^T}{\partial \rho}\frac{\partial \mathbf{e}}{\partial \rho}}_{H_e} + \alpha\underbrace{\phi^2(g)\left(\frac{\partial g}{\partial \rho}\right)^2}_{H_g}. \tag{11}$$

From (10) and (11), it is clear that finding ρ^* in (8) with (9) requires the gradients $\partial\mathbf{e}/\partial\rho$ and $\partial g/\partial\rho$.

To derive the gradients with the aim to find ρ^*, the IFT algorithm is used as shown in Fig. 2. The algorithm consists of the following steps that only shortly will be addressed:

(1) Conduct three IFT experiments in the context of Fig. 1.
(2) Obtain the gradients $\partial J_e/\partial\rho$ and when coming from step (4) also compute the gradients $\partial J_g/\partial\rho$.
(3) With (9) compute the candidate parameter set ρ_{i+1}.
(4) Check if $g \leq \varepsilon$ with $\varepsilon > 0$, if satisfied, accept ρ_{i+1} and return to step (1), if not satisfied, proceed with step (2) to find a candidate parameter set ρ_{i+1} that does satisfy $g \leq \varepsilon$.

The IFT algorithm aims at obtaining unbiased estimates for the gradients $\partial\mathbf{e}/\partial\rho$. This will be explained in the remainder of this section by discussing the steps from Fig. 2 in more detail.

2.3 IFT experiments and the gradients $\partial\mathbf{e}/\partial\rho$

In view of Fig.1 consider three IFT experiments under identical point-to-point reference r and controller parameters ρ.

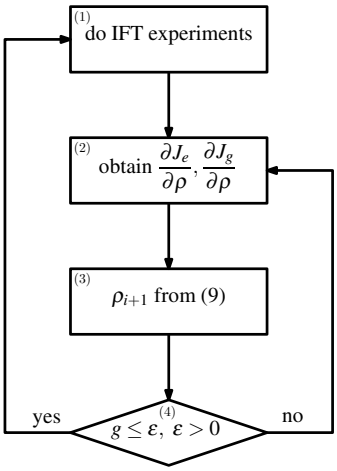

Fig. 2. Overview of the IFT algorithm.

Experiment 1 The result of the first experiment with no auxiliary input, i.e. $u_I = 0$, the subscript indicates the experiment number, satisfies the frequency-domain relation:

$$\begin{aligned} y_I(z) &= v_I(z) + \mathscr{P}(z)(\mathscr{C}_{ff}(z)r(z) + \mathscr{C}_{fb}(z)(r(z) - y_I(z)) \\ &= \mathscr{S}(z)v_I(z) + \mathscr{S}_c(z)\left(\frac{\mathscr{C}_{ff}(z)}{\mathscr{C}_{fb}(z)} + 1\right) r(z), \end{aligned} \tag{12}$$

with the sensitivity function $\mathscr{S} = \mathscr{S}(\omega, \rho)$ from (4) and the complementary sensitivity function $\mathscr{S}_c = \mathscr{S}_c(\omega, \rho)$ defined in frequency domain by

$$\mathscr{S}_c(z) = \frac{\mathscr{C}_{fb}(z)\mathscr{P}(z)}{1 + \mathscr{C}_{fb}(z)\mathscr{P}(z)}. \tag{13}$$

From the upper part in (12), it can be derived that

$$\frac{\partial y_I(z)}{\partial \rho} = \frac{1}{\mathscr{C}_{fb}(z)} \frac{\partial \mathscr{C}_{fb}(z)}{\partial \rho} \mathscr{S}_c(z)(r(z) - y_I(z)). \tag{14}$$

Given the fact that $e_I = r - y_I$, using (12) and (14) in (10) normally gives rise to a biased update for $\partial J_e/\partial \rho$ because the disturbances v_I contained in both $\mathbf{e}_I$ and $\partial \mathbf{e}_I/\partial \rho$ are correlated. Moreover, deriving the gradients using (14) requires a plant model in $\mathscr{S}_c$. To avoid bias in the gradient estimates, without the need for a plant model, multiple experiments are performed in the IFT algorithm, see Hjalmarsson [2002].

Experiment 2 Define the second experiment with the auxiliary input $u_{II} = e_I$, i.e. use the closed-loop error signal from the first experiment. The frequency-domain relation equals:

$$\begin{aligned} y_{II}(z) = \mathscr{S}(z)v_{II}(z) + \mathscr{S}_c(z)\left(\frac{\mathscr{C}_{ff}(z)}{\mathscr{C}_{fb}(z)} + 1\right) r(z) \\ - \mathscr{S}_c(z)e_I(z), \end{aligned} \tag{15}$$

Experiment 3 From a third experiment, which is similar to the first experiment, i.e. $u_{III} = 0$, obtain

$$y_{III}(z) = \mathscr{S}(z)v_{III}(z) + \mathscr{S}_c(z)\left(\frac{\mathscr{C}_{ff}(z)}{\mathscr{C}_{fb}(z)} + 1\right) r(z). \tag{16}$$

Subtracting (16) from (15) gives

$$\mathscr{S}_c(z)(r(z) - y_I(z)) = y_{III}(z) - y_{II}(z) + \mathscr{S}(z)(v_{II}(z) - v_{III}(z)), \tag{17}$$

or in view of the properties of the disturbances v,

$$\text{est}\{\mathscr{S}_c(z)(r(z) - y_I(z))\} = y_{III}(z) - y_{II}(z). \tag{18}$$

Substitution of (18) in (14) therefore gives an estimate of the gradients in (14):

$$\text{est}\left\{\frac{\partial y_I(z)}{\partial \rho}\right\} = \frac{1}{\mathscr{C}_{fb}(z)} \frac{\partial \mathscr{C}_{fb}(z)}{\partial \rho}(y_{III}(z) - y_{II}(z)), \tag{19}$$

which is based on measured data and known model relations regarding the controller $\mathscr{C}_{fb}(z)$. From (19) the step toward the gradients $\partial \mathbf{e}/\partial \rho$ is straightforward. From Fig. 1, it follows that

$$\frac{\partial e}{\partial \rho} = -\frac{\partial y}{\partial \rho}. \tag{20}$$

With (20) the gradients $\partial \mathbf{e}/\partial \rho$ are defined in time domain by

$$\frac{\partial \mathbf{e}}{\partial \rho} = -[\mathbf{C}_1(\mathbf{y}_{III} - \mathbf{y}_{II}) \dots \mathbf{C}_m(\mathbf{y}_{III} - \mathbf{y}_{II})], \tag{21}$$

with $\mathbf{C}_1 = \mathbf{C}(\rho), \dots, \mathbf{C}_m = \mathbf{C}_m(\rho)$ Toeplitz matrices containing the impulse responses of the (stable) filters

$$\mathscr{C}_m(z) = \frac{1}{\mathscr{C}_{fb}(z)} \frac{\partial \mathscr{C}_{fb}(z)}{\partial \rho_m}, \tag{22}$$

and the data-sampled signals $\mathbf{y}_{II} = [y_{II}(1) \dots y_{II}(N)]^{\mathrm{T}}$, with $\mathbf{y}_{II} = \mathbf{y}_{II}(\rho)$, and $\mathbf{y}_{III} = [y_{III}(1) \dots y_{III}(N)]^{\mathrm{T}}$, with $\mathbf{y}_{III} = \mathbf{y}_{III}(\rho)$.

In summary, experiment one provides $\mathbf{e} = \mathbf{e}_I$ and the auxiliary input for experiment two. The estimate of the gradients in (19) is obtained with experiment two and experiment three, i.e. having the disturbances v_{II} and v_{III}. Since v_{II} and v_{III} in $\partial \mathbf{e}/\partial \rho = \partial \mathbf{e}_{II,III}/\partial \rho$ do not correlate with v_I in $\mathbf{e}_I$, $\partial J_e/\partial \rho$ becomes unbiased. Note that this leaves the approximate Hessian matrix H_e in (11) biased. Unbiased estimates of the Hessian are investigated in Solari and Gevers [2004].

2.4 Computation of the gradient $\partial g/\partial \rho$

Computation of the gradient $\partial g/\partial \rho$ is done upon violation of the constraint $g > 0$, see Fig. 2. For the necessary violation detection a non-parametric model based on frequency response data is used for the sensitivity function $\mathscr{S} = \mathscr{S}(\omega, \rho)$ with the candidate parameter set $\rho = \rho_{i+1}$. Note that frequency response data measurements are inexpensive and quickly obtained, but cannot be used for controller synthesis, as model-based controller synthesis requires a parametric model. Furthermore, by imposing constraints, machine damage by using controller parameters that possibly induce severe violations of the closed-loop frequency-domain specifications will be avoided. In fact, no IFT experiments are done without reasonable assurance that the candidate parameter set $\rho = \rho_{i+1}$ found in step (3) of the IFT algorithm does not induce such violations.

To obtain the gradients $\partial g/\partial \rho$ from model prediction, i.e. the constrained part g, we use the center difference scheme:

$$\begin{aligned} \left.\frac{\partial g}{\partial \rho}\right|_{\rho=\rho_{i+1}} &= \left.\frac{\Delta g}{\Delta \rho}\right|_{\rho=\rho_{i+1}} + \mathscr{O}(\|h\|^2) \text{ for } \|h\| \to 0 \\ &\approx \left[\left.\frac{\Delta g}{\Delta \rho(1)}\right|_{\rho=\rho_{i+1}} \dots \left.\frac{\Delta g}{\Delta \rho(m)}\right|_{\rho=\rho_{i+1}}\right]^T, \end{aligned} \tag{23}$$

i.e. a perturbation method with step sizes $h = [h_1 \dots h_m]^{\mathrm{T}}$ where h is related to the controller parameters obtained per iteration i, i.e. $h_i = 0.01\rho_i$, and

$$\left.\frac{\Delta g}{\Delta \rho(j)}\right|_{\rho=\rho_{i+1}} = \frac{g(\rho(1) \dots \rho(j) + h_j \dots \rho(m)) - g(\rho(1) \dots \rho(j) - h_j \dots \rho(m))}{2h_j}. \tag{24}$$

To predict the effect of the gradient $\partial J_e/\partial \rho$ and approximate Hessian H_e coming from the unconstrained part e (and for

which we need to re-compute the candidate parameter set $\rho = \rho_{i+1}$) the fact is used that

$$\left.\frac{\partial J_e}{\partial \rho}\right|_{\rho=\rho_{i+1}} = \left.\frac{\partial J_e}{\partial \rho}\right|_{\rho=\rho_i} + H_e(\rho_i)\Delta\rho + \mathcal{O}(\|\Delta\rho^2\|) \text{ for } \|\Delta\rho\| \to 0, \tag{25}$$

with $\Delta\rho = \rho_{i+1} - \rho$, which implies

$$H_e|_{\rho=\rho_{i+1}} = H_e|_{\rho=\rho_i}, \tag{26}$$

see also Gevers [2002] for a similar approach. With (25), (26), and (23) substituted in (10) and (11) a new candidate set of the controller parameters $\rho = \rho_{i+1}$ is computed with (9). In an iterative way, we thus seek the set $\rho = \rho_{i+1}$ that satisfies $g \leq \varepsilon$ with $\varepsilon > 0$ a constant that can be chosen arbitrary small.

Remark 1 The unconstrained optimization problem in (8) is generally non-convex. With (9) it is therefore not realistic to expect more than local convergence, i.e. a sufficiently good initial parameter set ρ_0 is required. To ensure convergence the penalty $g \leq \varepsilon$ rather than $g \leq 0$ is used in the IFT algorithm of Fig. 2. Namely, even if exponential convergence would occur, it would take an infinite number of iterations to convergence from $g > \varepsilon$ toward the boundary $g = 0$. Contrarily, $g \leq \varepsilon$ may be reached in a finite number of steps. We thus accept a controlled violation of the frequency-domain robustness specifications by the amount of ε; a limited amount of violation seems anyway unavoidable since the estimate of the violation is done using model prediction. Replacing the penalty function g by a barrier function can partly solve for this problem but most likely at the cost of performance.

Remark 2 In the unconstrained optimization problem the time-domain part J_e is mixed with the frequency-domain part J_g. To scale both parts with respect to each other, the scaling factor α is chosen at $\alpha = 10$ nm^2. This is because $e \sim$ nm and $g \sim 1$ such that both parts J_e and J_g become equally weighted in (7). Similarly, the optimization window, i.e. the sampled data interval used to define J_e in (1), should be chosen with the application specifics in mind. For the stage control case, the data sampled signals $\mathbf{e}$ have $N = 500$ samples with 250 samples in the acceleration phase and 250 samples in the scanning phase of constant velocity, see Heertjes et al. [2010].

Remark 3 An important aspect in the optimization algorithm is the choice of the iteration factor γ_i. The strategy that is followed is to start with $\gamma_0 = 1$ and then do a step refinement depending on the amount of violation encountered; see also Huusom et al. [2009].

3. STAGE CONTROL RESULTS

In terms of stage control results, this section has two parts: (a) the principles of wafer scanning and the properties of a wafer stage system will be addressed, and (b) results from IFT obtained with a 4th order simulation model and experimental results obtained from an actual wafer stage system will be discussed. It is emphasized that the model is used only for simulation purposes. IFT does not require a plant model.

3.1 Wafer scanners

Consider the schematics of a wafer scanner in Fig. 3 where (extreme) ultraviolet light containing an image of the integrated circuits to be processed travels via a light path through an optical column to expose the light sensitive layers of a wafer. The image is obtained from the reticle which is part of the reticle stage motion control system. Similarly, the wafer is part of the wafer stage motion control system. During wafer scanning both the reticle and the wafer stage systems track a series of point-to-point motions in (scanning) y-direction.

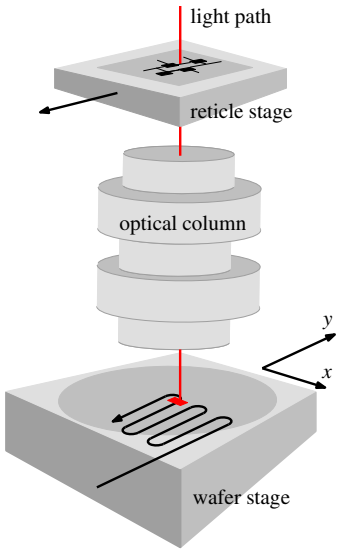

Fig. 3. Schematics of a wafer scanner.

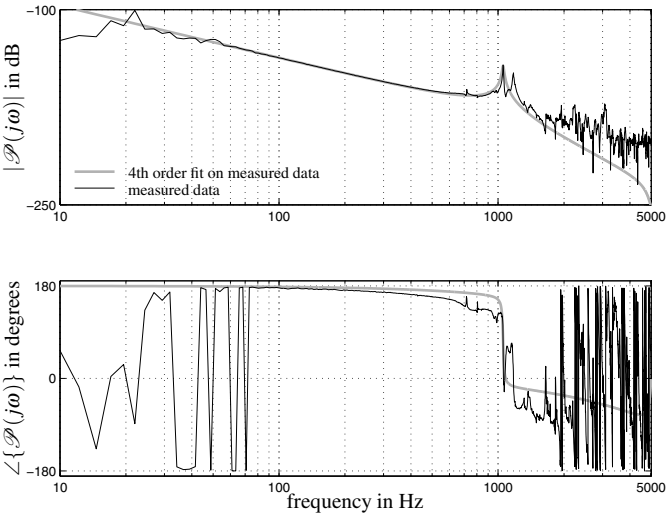

Fig. 4. Bode diagrams of the plant $\mathscr{P}$ with measured data and with a 4th order fit on these data.

If we consider the wafer stage system only, it can be seen in the Bode diagram representation of Fig. 3 by frequency response measurement that $\mathscr{P}$ essentially is a double-integrator based system. In addition, the result of a 4th order fit on the experimental data is shown. Given a zero order hold discretization scheme, the resulting parametric model equals

$$\mathscr{P}(z) = \frac{0.5z^{-2} + 0.5z^{-3}}{\beta(1 - 2\cos(\omega_n T)z^{-1} + z^{-2})(1 - 2z^{-1} + z^{-2})}, \tag{27}$$

with sampling time $T = 10^{-4}$ s, $\omega_n = 6.6\,10^3$ rad$\cdot$s^{-1}, and $\beta = 4.42\,10^9$ kg$\cdot$s^{-2}; in (27) the dimensionless damping $\zeta = 0.009$ is neglected.

To ease the notation, let us adopt the continuous-time representation. The wafer stage feedback controller $\mathscr{C}_{fb}$ has the following structure:

$$\mathscr{C}_{fb}(s) = \mathscr{C}_{PID}(s)\mathscr{C}_{LP}(s)\mathscr{C}_N(s), \tag{28}$$

with s the Laplace variable. The PID-controller part $\mathscr{C}_{PID}$, the low-pass part $\mathscr{C}_{LP}$, and the notch part $\mathscr{C}_N$ are given by

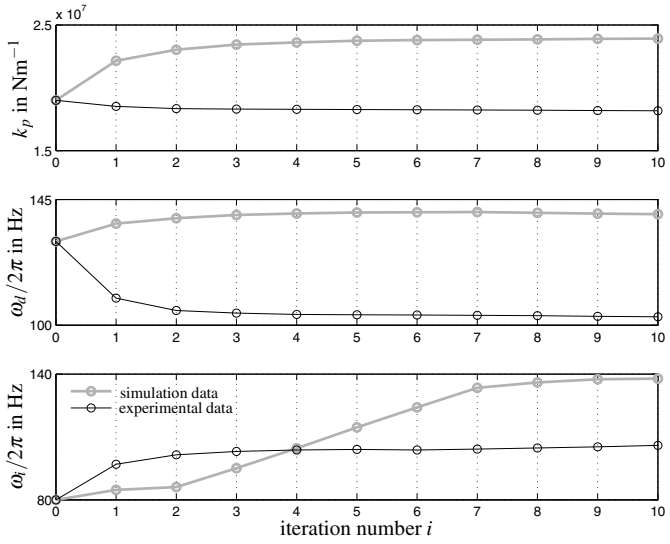

Fig. 5. IFT parameter convergence diagram either measured on a wafer stage or simulated with the 4th order model; $\mathscr{S}_b$ = 9.5 dB, $\alpha = 10$ nm^2, $\gamma_0 = 1$, ε = 0.5 dB.

$$\mathscr{C}_{PID}(s) = k_p\left(\frac{s}{\omega_d} + 1 + \frac{\omega_i}{s}\right),$$
$$\mathscr{C}_{LP}(s) = \frac{\omega_{lp}^2}{s^2 + 2\zeta_{lp}\omega_{lp}s + \omega_{lp}^2}, \text{ and } \mathscr{C}_N(s) = \prod_{i=1}^{n}\mathscr{N}_i(s), \tag{29}$$

with the notch filters

$$\mathscr{N}_i(s) = \left(\frac{\omega_{p,i}}{\omega_{z,i}}\right)\frac{s^2 + 2\zeta_{z,i}\omega_{z,i}s + \omega_{z,i}^2}{s^2 + 2\zeta_{p,i}\omega_{p,i}s + \omega_{p,i}^2}. \tag{30}$$

Since the 4th order model in Fig. 3 has only one resonance that possibly endangers closed-loop stability, one loop-shaping notch filter $\mathscr{N}_1$ is used in $\mathscr{C}_{fb}$ during simulations. Reversely, in the experiments, five notch filters $\mathscr{N}_1, \ldots, \mathscr{N}_5$ are used. The parameters of $\mathscr{C}_{LP}$ and $\mathscr{C}_N$ are fixed and are given in Tabel 1. Given the structure of $\mathscr{C}_{fb}$ in (28), IFT such as used in

$\mathscr{C}_{LP}$	ω_{lp} in rad $\cdot$ s^{-1}	ζ_{lp}	-	-
	$2\pi \cdot 1400$	0.80	-	-
$\mathscr{N}_i$	$\omega_{z,i}$ in rad $\cdot$ s^{-1}	$\zeta_{z,i}$	$\omega_{p,i}$ in rad $\cdot$ s^{-1}	$\zeta_{p,i}$
1	$2\pi \cdot 1100$	0.12	$2\pi \cdot 900$	0.20
2	$2\pi \cdot 430$	0.01	$2\pi \cdot 430$	0.03
3	$2\pi \cdot 718$	0.01	$2\pi \cdot 718$	0.05
4	$2\pi \cdot 812$	0.01	$2\pi \cdot 812$	0.03
5	$2\pi \cdot 1950$	0.01	$2\pi \cdot 1850$	0.05

Table 1. Fixed controller parameters of $\mathscr{C}_{fb}$.

this paper boils down to tuning the PID-controller parameters $\rho = [k_p\ \omega_d/2\pi\ \omega_i/2\pi]^{\mathrm{T}}$, see also Lequin et al. [2003].

In both simulation and experiment, the results of the IFT algorithm in terms of parameter convergence are depicted in Fig. 5. Given an identical set of default controller parameters ρ_0 at iteration number $i = 0$, it can be seen that convergence occurs in approximately ten iterations. The differences between the simulation data and the experimental data is mainly caused by the variation in disturbances and (plant) dynamics, hence the need for a different number of notch filters.

The comparison of the default parameter sets ρ_0 in Fig. 5 with the final parameter sets ρ_{10} in terms of the closed-loop sensitivity function $\mathscr{S}$ in (4) is shown in Fig. 6. For both the simulation data (top figures) and the experimental data (bottom figures), it can be seen that with IFT the final parameter sets at $i = 10$ induce improved low-frequency performance while satisfying

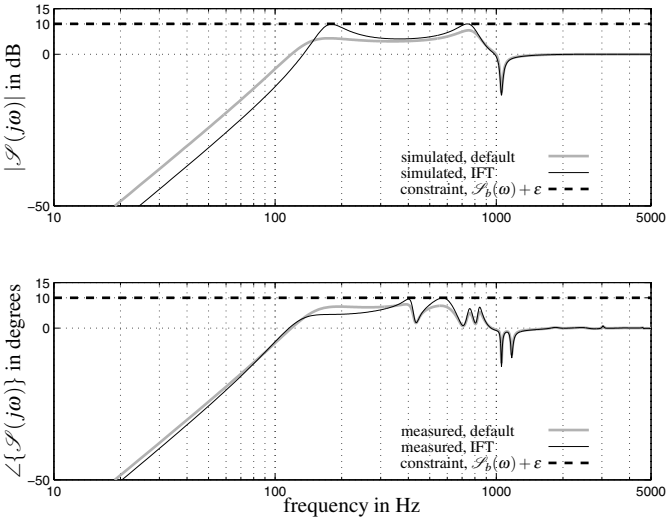

Fig. 6. Bode diagrams of the sensitivity function $\mathscr{S}$ either simulated with the 4th order model or measured on a wafer stage system and both without IFT (default) and with IFT; $\mathscr{S}_b$ = 9.5 dB, $\alpha = 10$ nm^2, $\gamma_0 = 1$, ε = 0.5 dB.

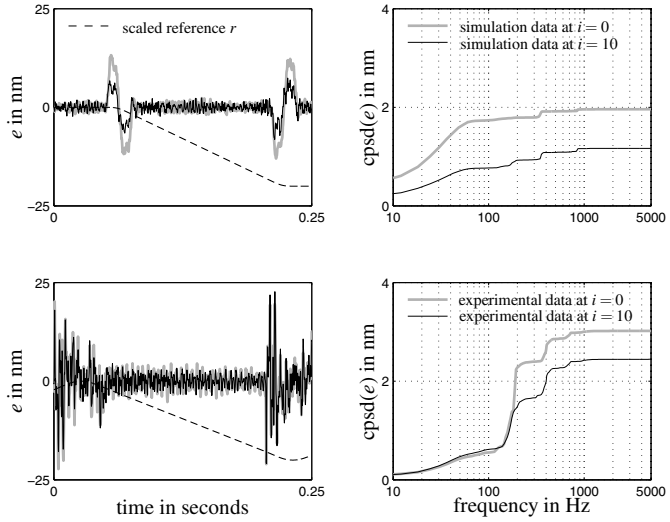

Fig. 7. Time-series simulation data and experimental data at iteration $i = 0$ and iteration $i = 10$ together with the results from cumulative power spectral density analysis.

the (indicated) amplitude constraints $\mathscr{S}_b(\omega) + \varepsilon$ at 10 dB. Note that the minor improvements shown at the bottom figure are clearly the result of the high industrial standards already met with the default controller set ρ_0. Furthermore, note that the amplitude constraints are approached at two distinct frequency points, which could favor the introduction of frequency-varying constraints. Regarding the loss of convexity properties in the posed optimization problem, see Heertjes et al. [2014] where local convexity properties are kept by tuning weighting filters, but which comes at the cost of posing hard constraints.

The effect of IFT in terms of time-domain performance is depicted in Fig. 7. Performance is evaluated regarding representative point-to-point motions (dashed curves). In the top figures simulation data is shown, whereas in the bottom figures experimental data is shown. The left part of the figure shows time-domain responses, whereas the right part shows a cumulative power spectral density analysis of these responses. In simulation, part of the improvements stem from reducing the error signals caused by a feed-forward mismatch. This part should be

handled by tuning an appropriate feed-forward controller $\mathscr{C}_{ff}$. In experiment, such a controller is present, see also Heertjes et al. [2010]. The improvement comes from a decreased level of amplification in the interval of constant velocity between 0.05 and 0.2 seconds, i.e. the performance interval where wafer scanning takes place. Decreasing the level of amplification in the frequency interval from 150 to 300 Hz, see Fig. 6, thus has a time-domain advantage that is identified by the IFT algorithm. This machine-specific advantage was unknown in advance and therefore not anticipated in the (manual) loop shaping tunings. This confirms the potential benefit of IFT to account for actual disturbance spectra in a control-relevant manner.

4. CONCLUSIONS

In this paper, a new approach for constrained IFT has been presented and experimentally demonstrated on an industrial high-precision stage system. The IFT algorithm is extended with a frequency-domain penalty to penalize violations of the frequency-domain specifications imposed on the closed-loop sensitivity function. Using a non-parametric model, an adaptation is made to the candidate parameter set obtained from IFT. The prediction involves a straightforward Taylor series expansion part using the resulting unbiased gradient estimates. Additionally, it involves a part that uses the perturbation method in obtaining the gradients with respect to the penalty. With the adaptation, a parameter set is obtained that from a model point of view meets the frequency-domain specifications. As a result, IFT is done under the assurance that frequency-domain specifications are either satisfied or violations of the specifications stay within controllable levels. For the PID controller parameters of a generally more advanced feedback controller structure, it is demonstrated that machine-specific performance, which is clearly disturbance-related, can be obtained with IFT. More specifically, IFT is used to create the machine-specific fine-tunings of the feedback control design in addition to the nominal loop shaping tuning process that is done in frequency domain. Tuning of the loop shaping filters themselves, which may prove even more beneficial, is left for future work.

ACKNOWLEDGEMENT

The authors gratefully acknowledge the fruitful discussions with and the contributions by Dragan Kostić and Bram de Jager. The work of the second author is supported by the Innovational Research Incentives Scheme under the VENI grant Precision Motion: Beyond the Nanometer (no. 13073) awarded by NWO (The Netherlands Organisation for Scientific Research) and STW (Dutch Science Foundation).

REFERENCES

A. Al Mamun, W.Y. Ho, W.E. Wang, and T.H. Lee. Iterative Feedback Tuning (IFT) of Hard Disk Drive Head Positioning Servomechanism. *In Proceedings of the Conference of the IEEE Industrial Electronics Society*, Taipei, Taiwan, 769-774, 2007.

F. Boeren, and T. Oomen. Iterative feedforward control: A closed-loop identification problem and a solution. *In Proceedings of the Conference on Decision and Control*, Florence, Italy, 2013.

M. Boerlage, M. Steinbuch, P. Lambrechts, and M. Van de Wal. Model-based feedforward for motion systems. *In Proceedings of the Conference on Control Applications*, 2003.

M.C. Campi, A. Lecchini, and S.M. Savaresi. Virtual reference feedback tuning: A direct method for the design of feedback controllers. *Automatica*, 38:1337–1346, 2002.

M. Gevers. A decade of progress in iterative process control design: from theory to practice. *Journal of Process Control*, 12(4):519-531, 2002.

A. Hansson, K. El-Awady, and B. Wahlberg A primal-dual interior-point method for iterative feedback tuning. *In Proceedings of the IFAC World Congress*, Beijing, China, 36–41, 1998.

M.F. Heertjes, D. Hennekens, and M. Steinbuch. MIMO feed-forward design in wafer scanners using a gradient approximation-based algorithm. *Control Engineering Practice*, 15(5): 495–506, 2010.

M.F. Heertjes, M. Galluzzo, and L. Kuindersma. Robust Data-Driven Control for the Stage Synchronization Problem. *IFAC World Congress*, Cape Town, South Africa, 1–6, 2014.

H. Hjalmarsson, S. Gunnarsson, and M. Gevers A convergent iterative restricted complexity control design scheme. *In Proceedings of the Conference on Decision and Control*, Lake Buena Vista, Florida, USA, 1735-1740, 1994.

H. Hjalmarsson. Iterative feedback tuning - An overview. *Journal of Adaptive Control and Signal Processing*, 16(5):373-395, 2002.

H. Hjalmarsson. From experiment design to closed-loop control. *Automatica*, 41:393-438, 2005.

J.K. Huusom, N.K. Poulsen, and S.B. Jørgensen. Improving convergence of iterative feedback tuning. *Journal of Process Control*, 19(4):570-578, 2009.

D. Kostić. Data-driven robot motion control design. *Ph.D. thesis*, Einhoven University of Technology, 2004.

O. Lequin, M.Gevers, M. Mossberg, E. Bosmans, and L. Triest. Iterative feedback tuning of pid parameters: comparison with classical tuning rules. *Control Engineering Practice*, 11(9):1023-1033, 2003.

D. Liu, A.J. McDaid, K.C. Aw, and S.Q. Xie. Position control of an ionic polymer metal composite actuated rotary joint using iterative feedback tuning. *Mechatronics*, 21(1):315-328, 2011.

S. Van der Meulen, R.L. Tousain, and O.H. Bosgra. Fixed structure feedforward controller design exploiting iterative trials: Application to a wafer stage and a desktop printer. *Journal of Dynamical Systems, Measurement, and Control*, 130:051006–1, 2008.

T. Oomen, R. Van Herpen, S. Quist, M. Van de Wal, O.H. Bosgra, and M. Steinbuch. Connecting system identification and robust control for next-generation motion control of a wafer stage. *IEEE Transactions on Control Systems Technology*, 22(1):102-118, 2014.

H. Prochazka, M. Gevers, B.D.O. Anderson, C. Ferrera. Iterative feedback tuning for robust controller design and optimization. *In Proceedings of the Conference on Decision and Control, and the European Control Conference*, Seville, Spain, 3602-3607, 2005.

Z.P. Rico, A. Lecchini-Visintini, and R.Q. Quiroga. Position control of an ionic polymer metal composite actuated rotary joint using iterative feedback tuning. *Mechatronics*, 21(1):315-328, 2011.

M.G. Safonov and T.C. Tsao. The unfalsified control concept and learning. *IEEE Transactions on Automatic Control*, 42(6):843–847, 1997.

G. Solari, and M. Gevers. Unbiased estimation of the Hessian for iterative feedback tuning. *In Proceedings of Conference on Decision and Control*, Paradise Island, Bahamas, 1759-1760, 2004.

S. Veres, and H. Hjalmarsson. Tuning for robustness and performance using iterative feedback tuning. *In Proceedings of the Conference on Decision and Control*, Las Vegas, Nevada, 4682-4687,2002.

P-H Yang, and S-L Koo. Control systems and methods applying iterative feedback tuning for feed-forward and synchronization control of microlithography stages and the like. *United States Patent*, US 8,451,431 B2, 2013.